Astronomy & Astrophysics manuscript no. nugas1
September 17, 2013

ALMA observations of feeding and feedback in nearby Seyfert galaxies: an AGN-driven outflow in NGC 1433 ⋆

F. Combes[1], S. García-Burillo[2], V. Casasola[3], L. Hunt[4], M. Krips[5], A. J. Baker[6], F. Boone[7], A. Eckart[8], I. Marquez[9], R. Neri[5], E. Schinnerer[10], and L. J. Tacconi[11]

[1] Observatoire de Paris, LERMA (CNRS:UMR8112), 61 Av. de l'Observatoire, F-75014, Paris, France e-mail: francoise.combes@obspm.fr
[2] Observatorio Astronómico Nacional (OAN)-Observatorio de Madrid, Alfonso XII, 3, 28014-Madrid, Spain
[3] INAF – Istituto di Radioastronomia & Italian ALMA Regional Centre, via Gobetti 101, 40129, Bologna, Italy
[4] INAF - Osservatorio Astrofisico di Arcetri, Largo E. Fermi, 5, 50125, Firenze, Italy
[5] IRAM, 300 rue de la Piscine, Domaine Universitaire, F-38406 Saint Martin d'Hères, France
[6] Dep. of Physics & Astronomy, Rutgers, the State University of New Jersey, 136 Frelinghuysen road, Piscataway, NJ 08854, USA
[7] CNRS, IRAP, 9 Av. colonel Roche, BP 44346, 31028, Toulouse Cedex 4, France
[8] I. Physikalisches Institut, Universität zu Köln, Zülpicher Str. 77, 50937, Köln, Germany
[9] Instituto de Astrofsica de Andalucía (CSIC), Apdo 3004, 18080 Granada, Spain
[10] Max-Planck-Institut für Astronomie (MPIA), Königstuhl 17, 69117 Heidelberg, Germany
[11] Max-Planck-Institut für extraterrestrische Physik, Giessenbachstr. 1, Garching bei München, Germany

Received 2013/ Accepted 2013

ABSTRACT

We report ALMA observations of CO(3-2) emission in the Seyfert 2 galaxy NGC 1433 at the unprecedented spatial resolution of $0\farcs5 = 24$ pc. Our aim is to probe AGN (active galactic nucleus) feeding and feedback phenomena through the morphology and dynamics of the gas inside the central kpc. NGC 1433 is a strongly barred spiral with 3 resonant rings: one at the ultra-harmonic resonance near corotation, and the others at outer and inner Lindblad resonances (OLR and ILR). A nuclear bar of 400 pc radius is embedded in the large-scale primary bar. The CO map, which covers the whole nuclear region (nuclear bar and ring), reveals a nuclear gaseous spiral structure, inside the nuclear ring encircling the nuclear stellar bar. This gaseous spiral is well correlated with the dusty spiral seen in HST images. The nuclear spiral winds up in a pseudo-ring at ∼200 pc radius, which might correspond to the inner ILR. Continuum emission is detected at 0.87 mm only at the very center, and its origin is more likely thermal dust emission than non-thermal emission from the AGN. It might correspond to the molecular torus expected to exist in this Seyfert 2 galaxy. The HCN(4-3) and HCO^+(4-3) lines were observed simultaneously, but only upper limits are derived, with a ratio to the CO(3-2) line lower than 1/60 at 3σ, indicating a relatively low abundance of very dense gas. The kinematics of the gas over the nuclear disk reveal rather regular rotation only slightly perturbed by streaming motions due to the spiral; the primary and secondary bars are too closely aligned with the galaxy major or minor axes to leave a signature in the projected velocities. Near the nucleus, there is an intense high-velocity CO emission feature redshifted to 200 km/s (if located in the plane), with a blue-shifted counterpart, at 2″ (100 pc) from the center. While the CO spectra are quite narrow in the center, this wide component is interpreted as an outflow, involving a molecular mass of 3.6 10^6 $M_\odot$, and a flow rate ∼ 7 $M_\odot$/yr. The flow could be in part driven by the central star formation, but mainly boosted by the AGN through its radio jets.

Key words. Galaxies: active — Galaxies: Individual: NGC 1433 — Galaxies: ISM — Galaxies: kinematics and dynamics — Galaxies: nuclei — Galaxies: spiral

1. Introduction

It is now observationally well established that supermassive black holes (SMBHs) reside in the nuclei of all galaxies with massive spheroids in the Local Universe and at higher redshifts as well (e.g. Kormendy & Ho 2013). Quasars at high redshift and Seyfert nuclei locally are fueled by accretion of material onto the SMBH. Although much progress has been made on both theoretical and observational fronts in the last decade, the relationship of black hole growth with galaxy formation and evolution is still far from being completely understood.

One of the outstanding problems is to identify the mechanism that drives gas from the disk towards the nucleus, removing its large angular momentum, to feed the central black hole and trigger the nuclear activity. Theoretically, broad-brush solutions have been found; cosmological simulations rely on merger-driven gas inflow via bar instabilities to feed a central starburst and fuel the SMBH (e.g., Hopkins et al. 2006; di Matteo et al. 2008). Nevertheless, in the Local Universe, no clear correlation has been found between the presence of an active galactic nucleus (AGN) and either companions or the presence of bars (see e.g. Combes 2003, 2006, Jogee 2006 for reviews). It is possible that locally the relation between these large-scale phenomena and the duty cycle of nuclear fueling is masked by different timescales. Indeed, the presence of resonant rings, vestiges of a previous bar, appears to be correlated with Seyfert activity (Hunt & Malkan 1999). Also it could be that gas inflow is not always possible because of dynamical barriers (e.g., nuclear rings, see Piner et al. 1995; Regan & Teuben 2004).

Send offprint requests to: F. Combes
⋆ Based on observations carried out with ALMA in Cycle 0.

To assess potential inhibitors of the ubiquitous gas inflow assumed in simulations, we must examine the nuclear kinematics around local AGN. This can be best done with molecular tracers, since in galaxy centers, HI is typically converted to molecular gas. CO line emission is therefore our best probe, and in particular CO(3-2), which traces the high density gas (10^4-10^5 cm^{-3}) in the dense AGN circumnuclear regions (as we have shown in Boone et al. 2011). HCN and HCO^+ line emission should trace the densest material (at least 10^7 cm^{-3}), and diagnose its excitation and chemistry. We have undertaken during the last decade the NUGA (NUclei of GAlaxies) program to study the gas distributions in nearby AGN, and find clues to their fueling. In the dozen nearby Seyfert or LINER galaxies observed with the IRAM Plateau de Bure interferometer (PdBI) in CO(2-1), we achieved a spatial resolution of 50-100 pc, and frequently worse for the most distant galaxies. In these galaxies, a large variety of gas distributions have been found; however we detected on-going AGN feeding at 0.1-1 kpc scales for only 5/12 cases: NGC 2782 (Hunt et al. 2008, bar triggered by an interaction), NGC 3147 (Casasola et al. 2008), NGC 3627 (Casasola et al. 2011), NGC 4579 (Garcìa-Burillo et al. 2009), and NGC 6574 (Lindt-Krieg et al. 2008). The most common feeding mechanism in these galaxies appears to be kinematically decoupled embedded bars, i.e. the combination of a slowly rotating kpc-scale stellar bar (or oval) and a kinematically decoupled nuclear bar, with overlapping dynamical resonances. Such resonances and kinematic decoupling are fostered by a large central mass concentration and high gas fraction. The gas is first stalled in a nuclear ring (a few 100 pc scale), and then driven inward under the influence of the decoupled nuclear bar. However, because of insufficient resolution, our previous observations were most of the time unable to probe the gas within 100 pc of the AGN.

In this paper, we present ALMA Cycle 0 observations in the CO(3-2) line of the Seyfert 2 NGC 1433, where the beam is 24 pc in size. The nearby distance (9.9 Mpc) and low inclination of 33° make NGC 1433 an ideal target to test and refine the scenario of AGN feeding and feedback, and constrain BH models which are only now beginning to examine in detail gas structures within 100 pc (Hopkins & Quataert 2010; Perez-Beaupuits et al. 2011).

Up to now, resolution of tens of pc scales has been obtained only in a few Seyfert galaxies, and only in hot or warm gas tracers. The best example is NGC 1068, the most nearby Seyfert 2 prototype, where near-IR H_2 lines have been mapped with SINFONI at 0.″075 resolution (5.2pc) by Müller-Sanchez et al. (2009). The behavior of this hot (1000-2000K) gas is not yet settled however; while an outflow model is proposed by Galliano & Alloin (2002), and a warped disk model by Schinnerer et al. (2000), Müller-Sanchez et al. (2009) propose a strong inflow model. Krips et al. (2011) explain their SMA CO(3-2) map at 0.″6 = 40 pc resolution by a rotating disk plus an outflow of the disk gas due to shocks and/or a circumnuclear disk-jet interaction. Thus, gas inflow could fuel the AGN at a 10-pc scale, and the jet-gas interaction could simultaneously drag gas outwards on scales of hundreds of pc. The presence of an outflow in the circumnuclear disk of NGC 1068 has also been suggested to be responsible of the large-scale molecular shocks revealed by strong SiO emission in this galaxy (Garcìa- Burillo et al 2010). The outflow is clearly seen in ALMA data (Garcìa-Burillo et al. 2013, in prep.). Typical outflow velocities are found of the order of 200 km/s in NGC 1068.

An important ingredient in cosmological simulations is feedback, which can regulate SMBH growth and suppress star formation (e.g., Croton et al. 2006, di Matteo et al. 2008, and references therein). Molecular observations can constrain specific feedback mechanisms, by discovering molecular outflows through their high velocity wings, and determine their origin (star formation or AGN), through high resolution observations. Chung et al. (2011) showed the ubiquitous presence of 1000 km/s molecular outflows in starbursts with SFRs larger than 100 $M_\odot$/yr (see also Feruglio et al. 2010, Fischer et al. 2010, Sturm et al. 2011). The CO emission in the high velocity wings may generally represent 25% of the total observed emission. In NGC 1068 the outflow, if present, is only of the order of 200 km/s and entrained by the radio jet. Coil et al. (2011) also find that galactic winds are frequent in ionized gas lines, in post-starburst and AGN host galaxies at 0.2<z<0.8, but they are low velocity winds, likely due to supernovae. High velocity winds, driven by an AGN, might be frequent in molecular gas (Leon et al. 2007, Feruglio et al. 2010, 2013, Alatalo et al. 2011, Nesvadba et al. 2011, Dasyra & Combes 2012, Aalto et al. 2012, Spoon et al. 2013, Veilleux et al. 2013), as well as in the ionized or atomic gas component (Rupke et al. 2005; Riffel & Storchi-Bergmann 2011). In Arp 220, Sakamoto et al. (2009) have discovered 100-200 km/s outflows, through P-Cygni profiles in HCO^+(3-2), HCO^+(4-3) and CO(3-2) along the line of sight to the nucleus. They interpret this gas as driven outwards by the nuclear starburst. Because NGC 1433 is not an IR-luminous starburst, it is unlikely that an AGN wind close to the nucleus would be swamped by a starburst wind, thus facilitating its identification with ALMA's high resolution.

Table 1. Basic data for the NGC 1433 galaxy

Parameter	Value[b]	Reference[c]
α_{J2000}[a]	$03^h42^m01.55^s$	(1)
δ_{J2000}[a]	-47°13′19.5″	(1)
V_{hel}	1075 km s^{-1}	(1)
RC3 Type	(R')SB(r)ab	(1)
Nuclear Activity	Seyfert 2	(2)
Inclination	33.°0	(3)
Position Angle	199° ± 1°	(3)
Distance	9.9 Mpc (1″ = 48 pc)	(4)
L_B	1.0×10^{10} $L_\odot$	(4)
M_{HI}	5.5×10^8 $M_\odot$	(5)
M_{H_2}	2.3×10^8 $M_\odot$	(6)
M_{dust}(60 and 100 μm)	2.5×10^6 $M_\odot$	(7)
L_{FIR}	1.3×10^9 $L_\odot$	(7)
α_{J2000}[d]	$03^h42^m01.49^s$	New center
δ_{J2000}[d]	-47°13′20.2″	New center

[a] (α_{J2000}, δ_{J2000}) is the phase tracking center of our ^{12}CO interferometric observations

[b] Luminosity and mass values extracted from the literature have been scaled to the distance of D = 9.9 Mpc.

[c] (1) NASA/IPAC Extragalactic Database (NED, http://nedwww.ipac.caltech.edu/); (2) Veron-Cetty & Veron (1986); (3) Buta et al. (2001); (4) HyperLeda; (5) Ryder et al. (1996); (6) Bajaja et al. (1995), reduced to the conversion factor 2.3 $10^{20}$$cm^{-2}$/(Kkm/s); (7) *IRAS* Catalog.

[d] New adopted center, coinciding with the continuum peak.

1.1. NGC 1433

NGC 1433 is a nearby active barred galaxy, member of the Dorado group which includes 26 galaxies (Kilborn et al. 2005). We selected it from a sample of low-luminosity AGN spirals already detected in CO emission, for its proximity, and moderate

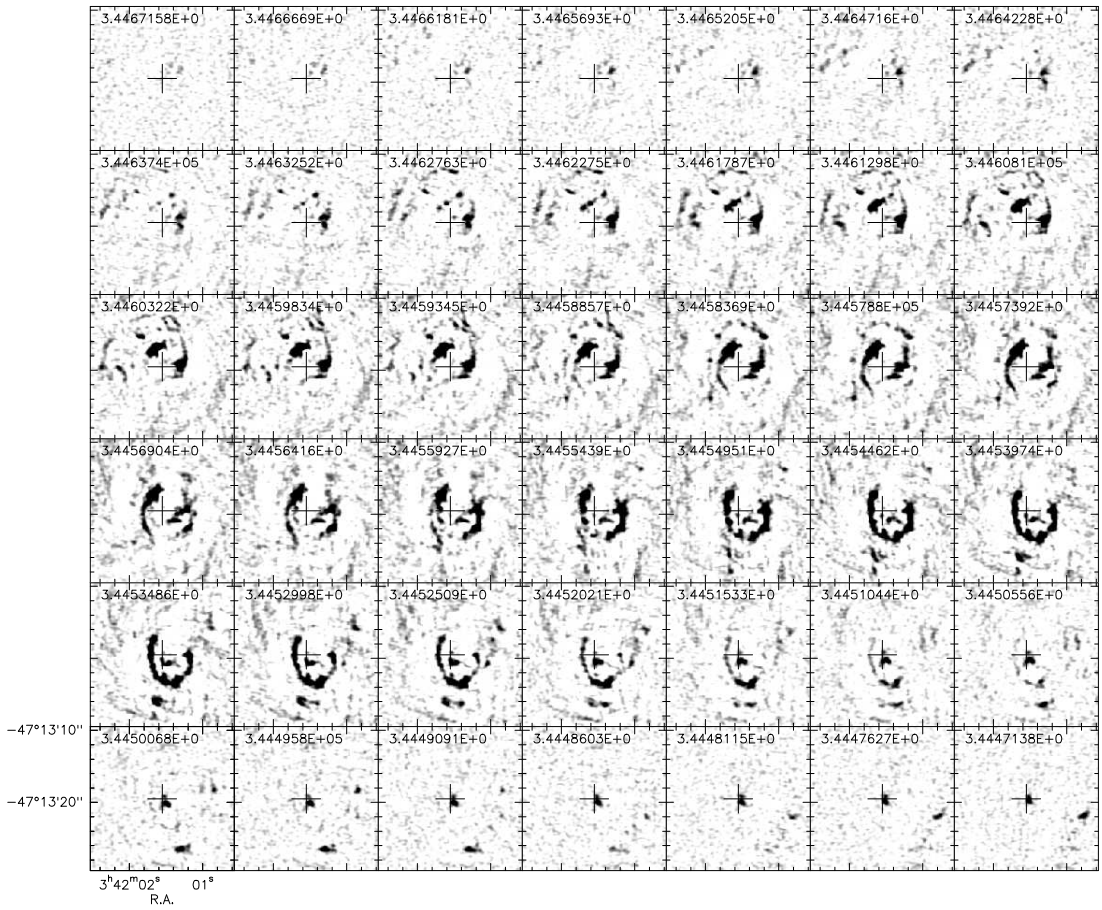

Fig. 1. Channel maps of CO(3-2) emission in the center of NGC 1433. Each of the 42 square boxes is 20″ in size, while the primary beam is 18″ in diameter . Channels are separated by 4.24 km/s. They are plotted from 978 (top left) to 1152 km/s (bottom right, the panels are labelled in frequency). The synthesized beam is 0.″56×0.″42 (PA=85°). The center of the maps is the phase center of the interferometric observations given in Table 1. The color scale is linear, between 1 and 30 mJy/beam.

Table 2. Main dynamical features in NGC 1433

Feature	Radius	PA(°)
Nuclear bar	9″ (430 pc)	31
Nuclear ring	9.5″ (460 pc)	31
Primary bar	83″ (4 kpc)	94
Inner ring	108″ (5.2 kpc)	95
Outer ring	190″ (9.1 kpc)	15

inclination. It has been classified as Seyfert 2 by Veron-Cetty & Veron (1986), for its strong nuclear emission lines and its high [NII]/Hα ratio. However, Sosa-Brito et al. (2001) prefer to classify it as LINER, because of its [OIII]/Hβ ratio, which is just at the limit between Seyfert and LINERs. Liu & Bregman (2005) detect the nuclear point source in X-rays with ROSAT.

The galaxy has a rich network of dusty filaments around the nucleus. Its morphology reveals conspicuous rings (Buta 1986, Buta et al. 2001); the presence of nuclear, inner and outer rings has motivated its nickname of the "Lord of Rings" (Buta & Combes 1996). Table 2 presents the sizes and orientation of the main dynamical features. NIR images have revealed a nuclear bar inside the nuclear ring, of radius ∼400 pc (Jungwiert et al. 1997). The ring is the site of a starburst and is patchy in UV (continuum HST image from Maoz et al. 1996). 31 compact sources contribute 12% of the UV light. Inside the ring the dust traces a flocculent or multiple-arm nuclear spiral structure (HST image from Peeples & Martini 2006). There is a peak of 6 mJy in radio continuum emission at 843 MHz in the center (Harnett 1987), with a weak extension along the bar. The HI 21cm emission map (Ryder et al. 1996) reveals that the atomic gas is concentrated in the inner and outer rings, with some depletion in the nuclear ring and bar region. In contrast, the central region is filled with molecular hydrogen (Bajaja et al. 1995, CO SEST map). Our ALMA single pointing includes in its field-of-view (FOV) all the nuclear bar and nuclear spiral gas.

2. Observations

The observations were carried out with the Atacama Large Millimeter/submillimeter Array (ALMA) telescope in Cycle 0, with 19 antennae, during june and july 2012. NGC 1433 was observed simultaneously in CO(3-2), HCO^+(4-3), HCN(4-3), and continuum, with Band 7. The sky frequencies were 344.56 GHz, 355.46 GHz, 353.24 GHz and 343.27 GHz respectively. The observations were done in 3 blocks, with a total duration of 2 hours. For each period, NGC 1433 was observed for 27 minutes; the median system temperatures were T_{sys} = 140, 230 and 160 K.

The observations were centered on the nucleus, with a single pointing covering a FOV of 18″. The Cycle 0 extended configuration provides in Band 7 a beam of 0.″56×0.″42, with a PA of 85°. The galaxy was observed in dual polarization mode with 1.875 GHz total bandwidth per baseband, and a velocity resolu-

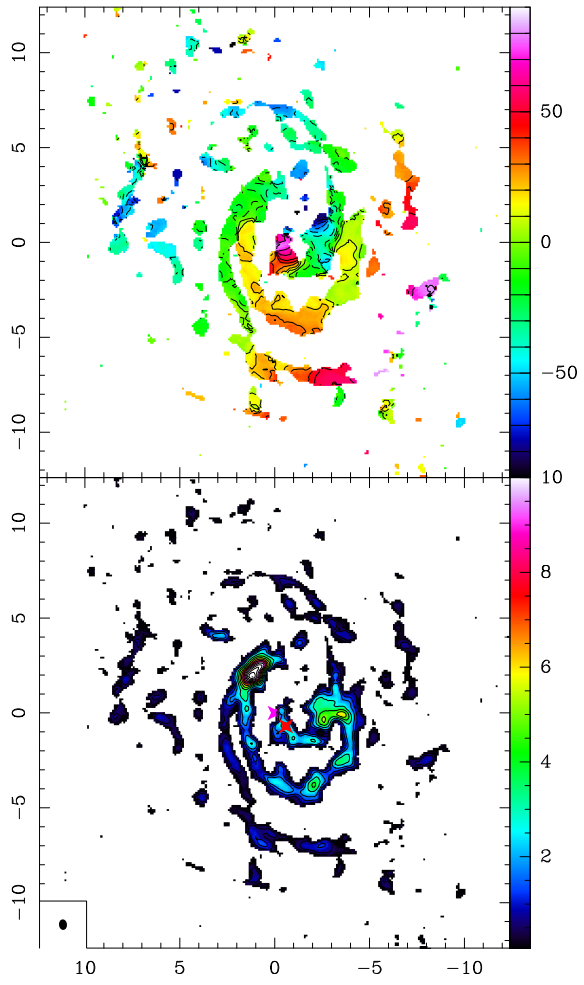

Fig. 2. Velocity field (top) and integrated intensity (bottom) of the CO(3-2) emission in the center of NGC 1433. Coordinates are RA-Dec in arcsec relative to the phase center (see Table 1). The color scale ranges are in km/s relative to 1075 km/s (top) and in Jy/beam.MHz (or 0.87 Jy/beam.km/s) at the bottom. The beam size of 0.″56×0.″42 is indicated at the bottom left. The phase center is a pink cross, and the new adopted center is the red cross, in the bottom panel.

tion of 0.488 MHz ~0.42 km/s. The spectra were then smoothed to 4.88 MHz (4.24 km/s) to build channel maps.

This choice of correlator configuration, selected to observe simultaneously three lines, provided a velocity range of 1600 km/s for each line, but not centered (200km/s on one side and 1400 km/s on the other) which is adequate for a nearly face-on galaxy, and 1800 MHz bandwidth in the continuum. The total integration time provided an rms of 0.09 mJy/beam in the continuum, and ~3 mJy/beam in the line channel maps (corresponding to ~170 mK, at the obtained spatial resolution). The flux calibration was done with the nearby quasar J0334-401, which is regularly monitored at ALMA, and resulted in 10% accuracy.

The data were calibrated, and cleaned using first a mask at the 50 mJy emission level, and then the 30 mJy level. The final cube has 360x360 pixels with 0.″1 per pixel in the plane of the sky, and 60 channels of 4.24 km/s width. The data were calibrated, imaged and cleaned with the CASA software (v3.3; McMullin et al. 2007), and the analysis was then finalized with the GILDAS software (Guilloteau & Lucas 2000).

The final maps were corrected for primary beam attenuation to compute fluxes, but were kept uncorrected for the plots.

Table 3. CO(3-2) line fluxes, after primary beam correction

Line	S_{CO} Jy km/s	V_{hel} km/s	$\Delta V^{(1)}$ km/s	Peak flux Jy
Total	234± 1	1073.1±0.3	85.3± 0.7	2.58
C1	103± 2	1040.0±0.4	46.± 1	2.1
C2	105± 4	1089.1±0.2	30.± 1	3.3
C3	26± 3	1123.0±4.0	59.± 5	0.4
Blue[(2)]	6.0± 0.1	1018.7±0.6	61.± 1	0.09
Red[(2)]	10.1± 0.1	1138.2±0.3	56.± 0.7	0.17

Total = Gaussian fit, assuming only one component, C1/C1/C3 represent 3 velocity-component decomposition
(1) Full Width at Half Maximum FWHM
(2) Fits for the blue and red components of the outflow, summed over a region 0.″7×1.″2 each (cf Fig 9).

Almost no CO(3-2) emission was detected outside the Full-Width Half-Power (FWHP) primary beam. Due to missing short spacings, extended emission was filtered out at scales larger than ~3″ in each channel map. The elongated features detected, corresponding to the dust lanes, along arms and rings are, however, quite narrow (thinner than 2″ as in HST images), so the missing-flux problem might not be severe in individual velocity slices. Low level negative sidelobes adjacent to bright emission were however observed.

3. Results

Figure 1 displays 42 of the CO(3-2) channel maps, with a velocity range of 175 km/s and a velocity resolution of 4.24 km/s. The velocity field is rather regular, although perturbed by the tightly-wound spiral structure (see also Fig. 2). At the outermost channels, the emission at the highest velocities does not occur primarily at large radii, but mainly towards the center.

3.1. Molecular gas distribution and morphology

To measure fluxes we used a clipped cube where all pixel values <2σ (6 mJy/beam) were set to zero. The mean intensity is plotted in Fig. 2 (bottom). Since the galaxy is more extended than the primary beam, it is difficult to quantify the missing flux. We compare to the central spectrum obtained with a single dish in Sect. 3.4. However, these observations were obtained with the SEST in CO(1-0) with a 43″ beam. Nevertheless, our FOV encompasses the entire nuclear ring, and the emission in this nuclear region has by far the strongest surface density at many wavelengths (Buta et al. 2001, Comeron et al. 2010; Ho et al. 2011).

We superposed the CO map onto the HST maps in the B, V and I filters. All show a remarkable similarity in morphology, as displayed in Figure 3. The features are so distinct that they were used to align the HST images, which suffered from an inexact astrometry. The CO emission nicely corresponds to the dust lanes, interleaved with the bright regions. The gas and the dust are intimately mixed, and reveal a multi-arm structure with a low pitch angle. There is not a well-defined density-wave here, but rather a more flocculent spiral structure with multiple branches. The structure is easily appreciated, thanks to the low inclination of the galaxy (33°, Table 1). This spiral structure is entirely included inside the nuclear ring, of ~ 10″=0.5 kpc in radius (Buta et al. 2001, see Table 2).

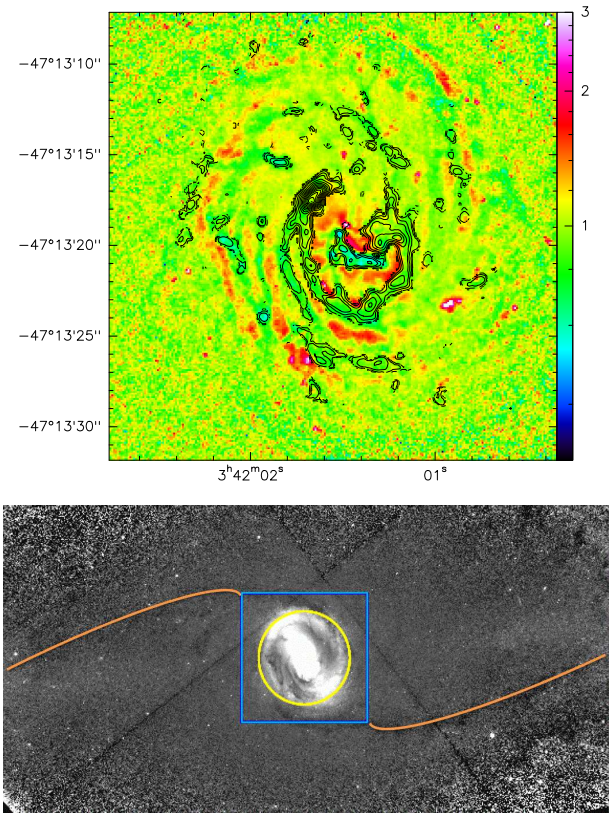

Fig. 3. *Top*: Overlay of CO(3-2) contours on the unsharp-masked blue (F450W) HST image. The HST image has been aligned to correspond to the ALMA astrometry. *Bottom:* Unsharp masking of the HST I-image of NGC 1433, covering the nuclear ring and the dust lanes along the primary bar. The FWHP of the primary beam is indicated in yellow (18″ in diameter), and the FOV of the CO map in Fig. 2 and in the above image is indicated in blue (square of 24.″8 on a side). The characteristic dust lanes on the leading edge of the main bar are outlined in orange.

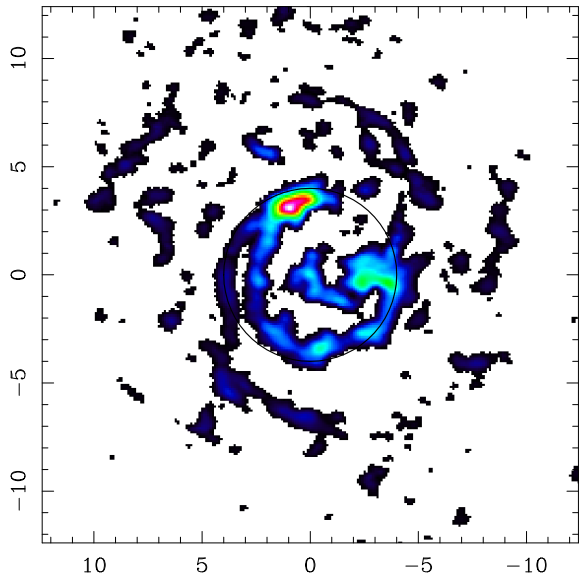

Fig. 4. Deprojection of the CO emission towards a face-on disk, centered on the new adopted center of Table 1. The pseudo-ring of 4″ radius, here underlined with a black circle, is standing out, nearly round.

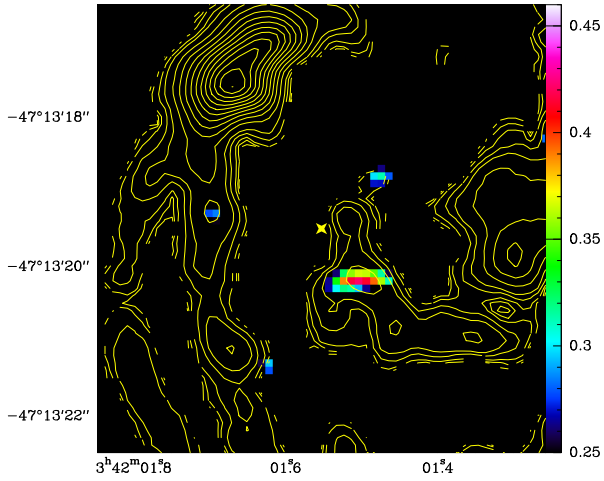

Fig. 5. Overlay of CO(3-2) contours on the 0.87mm continuum image. The FOV is 6″ in diameter. The yellow star shows the phase center of Table 1, while the peak of the continuum is our new adopted center. The colour palette unit is mJy.

What is remarkable is the large difference between the gas complex morphology in this nuclear region, revealed by ALMA and the already known smoother stellar morphology (Buta et al. 2001). The lower panel of Fig. 3 shows an unsharp-masked red image of the nuclear region, embedded in the primary bar whose leading dust lanes are marked. As is frequently found in strong primary bars of early-type spirals, the dust lanes wind up onto the nuclear ring, which corresponds to the inner Lindblad resonance, and a secondary nuclear bar has decoupled inside (e.g. Buta & Combes 1996). However, the gas does not follow the stellar nuclear ring, but instead is flowing through a flocculent spiral onto an even smaller nuclear ring, of ∼200pc radius, and from there reaches the very center, at least at the 20pc scale, our resolution.

The molecular gas morphology reveals notable asymmetries: for instance the peak of CO emission is not in the center but in a NE cloud complex, at about 4″ from the center (200 pc), with no SW counterpart. In the very center, the emission extends 2″ to the SW, but with a corresponding hole in the NE. This might indicate an $m = 1$ Fourier component, in addition to the $m = 2$ and $m = 3$ arm features. To determine whether one particular m component dominates, we have computed the Fourier decomposition of the 2D gas density, once the galaxy disk has been deprojected to the sky plane [1]. Fig. 4 displays the face-on molecular gas distribution. The pseudo-ring at radius ∼4″ corresponding to 200 pc is clearly visible and nearly round. We have computed the radial distribution of the various Fourier components, normalized to the axi-symmetric power. The surface density of the gas has been decomposed as:

$$\Sigma(r,\phi) = \Sigma_0(r) + \sum_m a_m(r) cos(m\phi - \phi_m(r))$$

and the amplitude of the various Fourier components m are normalized as $A_m(r) = a_m(r)/\Sigma_0(r)$. As a result, all $A_m(r)$ coefficients show noisy behaviours, at a maxium amplitude of 0.5, but there is no particular dominance of any m feature.

[1] The decomposition is performed using the new center defined in Sect. 3.2.

3.2. Continuum emission

Besides the CO(3-2) line, continuum emission was detected at 0.87mm. For that, the fourth band of width 468.8 MHz was used, with a rms noise level of 0.15 mJy. Fig. 5 displays the CO(3-2) contours superposed onto the continuum map. The peak emission is just detected at 3σ, about 0.5 mJy. The emission is extended in the East-West direction, its size is 1″x 0.″5.

3.2.1. Recentring

To establish the origin of the continuum emission, one issue is to determine the exact position of the AGN. We observed with a phase center corresponding to the peak of the near-infrared emission of the stellar component, which is known only within 0.″7 uncertainty (e.g. 2MASS catalog, 2003). The HST maps, in B, V and I would be precise enough, but they are all affected by dust obscuration. In particular there is a conspicuous dust-lane extending nearly horizontally in the SW. The continuum emission peaks at a position (-0.″6, -0.″7) with respect to our phase center, so perfectly compatible within the uncertainty. This position is however better centered with respect to the CO emission. We therefore choose to adopt the peak of the continuum emission as the new center. The latter is also perfectly compatible with the position of the X-ray nuclear point source seen by Liu & Bregman (2005). Although the AGN might not correspond exactly to the peak of the stellar component, it is possible that our new center is also the correct position of the AGN and the supermassive black hole. But it is unclear whether or not the 0.87 mm AGN synchrotron emission is detected.

3.2.2. Slope of radio-continuum emission

Radio continuum emission has been detected at 35 cm by Harnett (1987) with a resolution of 43″×58″; the emission is extended, and shows 6 mJy in the central beam. NGC 1433 has also been observed at 21 cm with ATCA by Ryder et al. (1996), with a spatial resolution of 30″. The central emission is 3.4 mJy, quite similar to what is obtained at the ends of the bar from the HII regions. Since the whole nuclear region is included in their central beam, it is possible that all the radio emission comes from star formation in the ring or nuclear region (both synchrotron from supernovae, and free-free emission). The continuum becomes 2 mJy at 4.8 GHz, with no polarisation (Stil et al. 2009). Comparing the central fluxes at 21cm and 0.87mm, the slope of the radio spectrum would be -0.35, which could be a mixture of synchrotron with a steeper spectrum (-0.7), and free-free emission with slope -0.1. Both steep radio spectra (Sadler et al. 1995), and flat ones (Ulvestad & Ho 2001) have been found in Seyfert spiral galaxies, so it is not possible to conclude on the AGN contribution in the center. From the Hα flux it would be possible in principle to estimate the fraction of free-free emission expected in the center, but the spatial resolution (2″) is not enough to disentangle what is coming actually from the very center. Also the extinction might be a problem.

3.2.3. Dust continuum emission

Another possibility is that the continuum is coming from thermal dust emission. At millimeter wavelengths, we are nearly in the Rayleigh-Jeans domain, and the dust emission is only proportional to the dust temperature. Continuum dust emission is then expected to be quite similar in morphology to the CO(3-2) emission (e.g. Dumke et al. 1997). Why is this not the case? The difference might be due to the lack of short spacing data, and the filtering out of the diffuse extended continuum emission. Indeed, the continuum is much more sensitive to this problem than the line emission. From the IRAS fluxes, the average temperature of the dust in NGC 1433 can be estimated as 24 K, assuming that the dust opacity has a dependence in frequency of ν^{β}, with $\beta = 2$. This is similar to central dust temperatures observed in ∼40″ beams with *Herschel* in star-forming barred galaxies such as NGC 3627 (Hunt et al. 2013, in prep.). From a flux of 0.5 mJy/beam, and assuming the same Draine & Lee (1984) dust absorption cross section as described in Dumke et al. (1997) for a solar metallicity, we find a molecular gas column density of $N(H_2) = 4.5\ 10^{22}$ cm^{-2}, over a beam of 24 pc in size. This is what is expected from a typical Giant Molecular Cloud. In comparison, in the same position, the CO(3-2) emission is about 4 Jy km/s, for a CO integrated intensity in one beam of 262 K km/s, corresponding to $N(H_2) = 6\ 10^{22}$ cm^{-2}, with a standard conversion factor of $2.3\ 10^{20}$ cm^{-2}/(K km/s) (e.g. Solomon & Vanden Bout 2005). Considering all the uncertainties, the continuum emission is at the level expected from dust alone. Given that dust emission is only detected at the very center, it might be possible that this dust is associated with the molecular torus expected to hide the AGN in this Seyfert 2 galaxy. The derived mass of the torus would be $9\ 10^5$ M$_\odot$. Since the dust in the torus is certainly warmer than in the disk, this might also explain why the continuum emission is not more extended, like the CO, in addition to the interferometer's filtering argument explained above. Mid-infrared maps with ISO at 7 and 15μm show also a high central concentration, but with low resolution (Roussel et al. 2001).

Only high-resolution observations with ALMA at several different frequencies would be able to settle the origin of the continuum emission, and determine whether the AGN is detected directly.

3.3. CO kinematics: a molecular outflow?

In a previous paper (Buta et al. 2001), a detailed mass model of NGC 1433 has been performed, from NIR photometry and Hα spectroscopy. Rotational and epicyclic frequencies (Ω and κ) were then derived, and together with the numerical simulations from Buta & Combes (2000), the predictions of the resonance locations, compared to the observed ring radii, favored a pattern speed of 23 km/s/kpc (or 26 km/s/kpc with our slightly different distance adopted). With this pattern speed, there are two inner Lindblad resonances (ILRs), located at 3.6 and 30″[2]. The existence of two ILRs weakens the primary bar, and allows the decoupling of a secondary bar, with a higher pattern speed (e.g. Friedli & Martinet 1993, Buta & Combes 1996). The nuclear bar produces negative torques on the gas, previously stalled at the nuclear ring, and provides a dynamical way to fuel the nucleus. This process has been simulated in detail in Hunt et al. (2008), and shows how the gas in the nuclear ring progressively flows to the center, in a spiral structure, and in a ring shrinking in radius. It appears that this scenario applies quite well to NGC 1433: its nuclear ring lies between the two ILRs, and the molecular gas morphology reveals an accumulation of the gas at the inner ILR. This configuration strongly suggests that the gas is presently fueling the AGN.

The top panel of Figure 2 displays the velocity field of the molecular gas. The velocity field is well described by rotation,

[2] Treuthardt et al. (2008) propose a lower value for the pattern speed in NGC 1433, 18 km/s/kpc, but their simulation shows a nuclear ring much larger in size than observed.

with the same position angle as the HI velocity field at larger scales (Ryder et al. 1996) and consistent with the Hα central kinematics (Buta et al. 2001). There are no strong perturbations to this regular rotation due to streaming motions in a barred potential, since the major axis of the galaxy is aligned with the minor axis of the primary bar, and also with the nuclear bar (see Fig. 3). The amplitude of the rotation is low but compatible with the observed Hα velocities within 10″ in radius, given the low inclination of 33°. The rotation velocities deduced from the CO kinematics are plotted in comparison to the Hα rotation curve in Fig. 6.

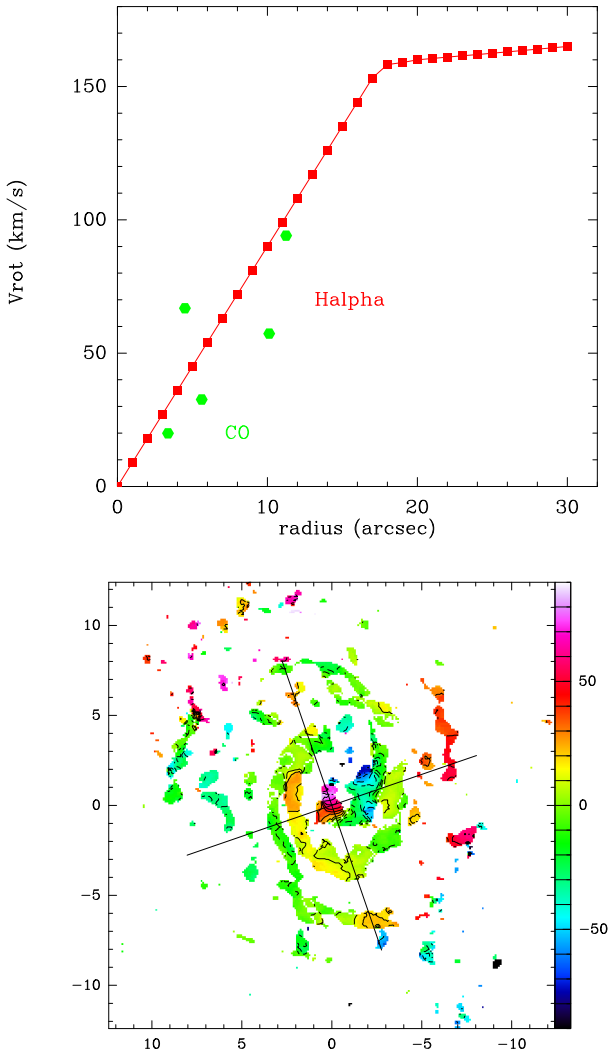

Fig. 6. *Top*:Rotational velocity model adopted for NGC 1433, based on the Hα kinematics (red filled squares) from Buta et al. (2001), compatible with the CO rotation curve (green filled hexagons). The CO velocity field is however sparsely sampled. *Bottom*: Velocity residuals after subtraction of a regular rotation model, based on the Hα rotation curve above. The map has been recentered on the new adopted center of Table 1. The two orthogonal lines indicate the position of the PV diagrams of Fig 7.

There is however a noticeable redshifted perturbation located in the very center and extending to the south-west between 0 and 2″ i.e. 100 pc in extent. To better isolate this feature, we plot the position-velocity diagram along the major axis of the galaxy in the top of Fig. 7. This slice reveals gas jumping by almost 100 km/s in projection, at much higher velocity than the rest of the nuclear disk gas. There is also a noticeable blue-shifted counterpart, at a distance from the center of about 2″ (100 pc) towards the north-west, which is conspicuous in the position-velocity diagram along the minor-axis of the galaxy in the bottom of Fig. 7. In this direction, both flow components are seen, while the largest gradient of velocities is along PA= 135°, which might be the projected direction of the flow.

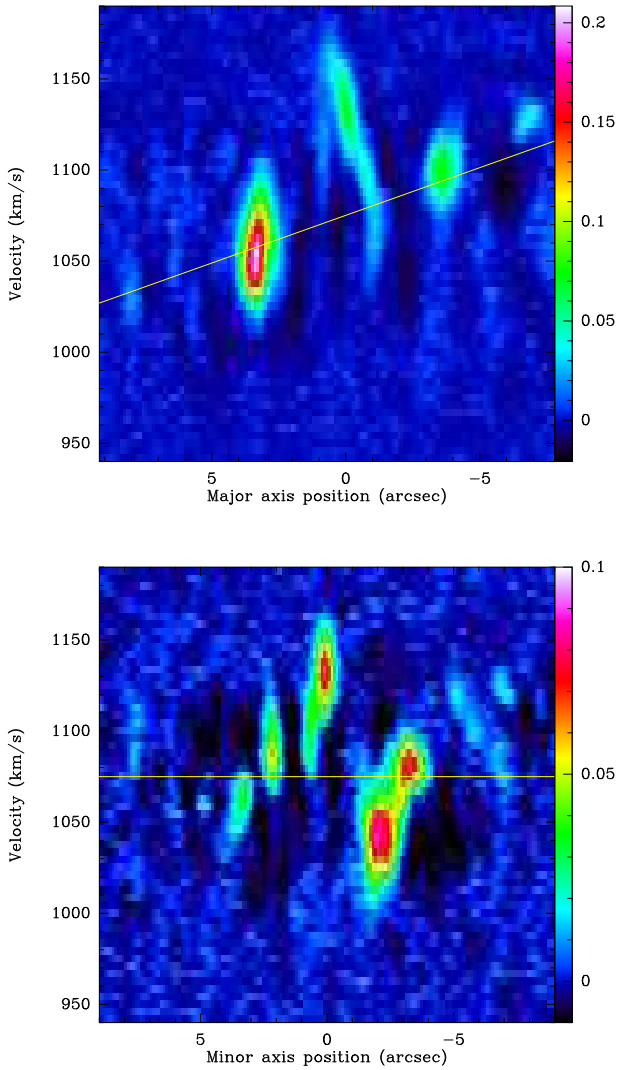

Fig. 7. *Top*: Position-velocity diagram along the major axis of PA = 199° (east is at left). The central outflow is clearly visible superposed on the smooth rotational velocity gradient (underlined by the yellow line, corresponding to the rotation curve of Fig. 6). *Bottom*: Position-velocity diagram, along the minor axis, of PA = 109° (East is at left). The two components (red and blue) of the outflow are visible, along a slice, where the velocity should be equal to the systemic one (yellow line).

Another way to compare these peculiar velocities to the rest of the nuclear region in 2D, is to subtract the expected regular velocity field known from the Hα gas in the same region. Fig. 6 displays the residuals obtained, relative to the adopted Hα rotation curve, plotted above. The figure shows the ionized gas

rotation curve deduced by Buta et al. (2001). The derived CO velocities, although in sparse regions, are compatible with this adopted rotation curve. The stellar velocity, once corrected by a large asymmetric drift, appears higher (Buta et al. 2001). The gas then does not follow the maximum circular velocity. This might be due to substantial gas turbulence, and/or to an overestimation of the correction of the stellar velocity.

The peculiar velocity of the gas at the nucleus and northwest of the center is clearly seen in the residuals of Fig. 6. If the gas were in the plane, the deprojected velocity could be as high as 200 km/s, but other orientations with respect to the sky plane are possible. Let us call α the angle between the outflow direction and the line of sight. The observed velocity in projection is $V_{outflow}\cos(\alpha)$, and the extend of the flow in the plane of the sky is $R_{outflow}\sin(\alpha)$. It is likely that α is not close to the extreme values, i.e. zero or 90 degrees, since the observed outflow velocity and the projected size of the outflow are both subtantial, i.e. respectively ~ 100 km/s and ~ 100 pc. This means that $\tan(\alpha)$ is of the order of 1. The flow is aligned roughly with the minor axis, and if it was orthogonal to the plane, $\tan(\alpha)$=0.6. We think, however, that the outflow is not orthogonal, since we are seing the galaxy inclined by 33° on the sky, and the near side is the NW, from the winding sense of the spiral arms, assumed trailing. The outflow cannot be exactly perpendicular to the disk, unless the blue and red regions would be inverted. The flow must at least be inclined by an angle > 33° from the normal to the plane. Conservatively, the outflow velocity likely lies between 100 km/s and 200 km/s.

This high-velocity gas is also noticeable in the total spectrum, obtained by summing the signal over the field-of-view, as in Fig. 8. A Gaussian decomposition in three components has been performed on the spectrum, and the results displayed in Table 3. The high-velocity red component represents nearly 5% of the total. The blue-velocity counterpart is diluted in the normal rotational component C1 (part of the two-horn profile characteristic of rotation).

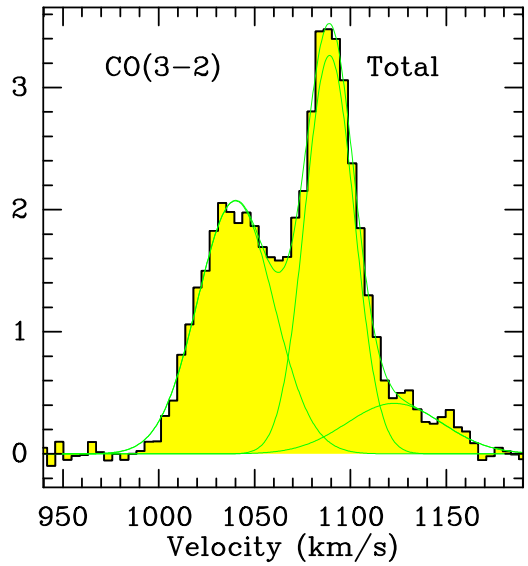

Fig. 8. Total CO(3-2) spectrum, integrated over the observed map, with a FOV of 18″, after correction for primary beam attenuation. The vertical scale is in Jy. The green line is the result of the Gaussian fit with 3 velocity components; see Table 3.

Finally, the high-velocity red component is best located in the map through the individual spectra of Fig. 9, where all spectra are shown within a radius of 2.″5. Although in principle, this high velocity gas could be inflowing as well as outflowing, we consider inflow to be unlikely. Indeed, there is no other signature of violent perturbation due to a companion nearby, and if gas were slowly accreted to fuel the AGN, it would first have settled into the rotational frame at much larger radii than the last 100 pc.

To better estimate the quantity of gas in the outflow, we have summed the CO flux within 2 regions of sizes 0.″7×1.″2, centered on the red and blue outflow regions, taking into account the primary beam correction (cf Fig 9). The results are given in Table 3. Assuming the standard CO-to-H_2 conversion factor (see next Section). we derive molecular masses of 1.3 10^6 and 2.3 10^6 M⊙ for the blue and red velocity components, respectively.

Is the outflow also detected in the ionized gas? There is no outflow detected in X-rays, but there is not enough spatial resolution to see it anyway. In Hα maps and spectroscopy, it is hard to reach a conclusion, even from the best velocity field obtained from Fabry-Perot interferometry by Buta (1986). In his Fig. 8, we can see a quite perturbed velocity field inside the central 20″, which may reflect steep gradients. However, the spatial resolution is only 2″, while the projected distance between our red and blue outflow peak components is roughly the same. An outflow of ionized gas is however quite compatible with the data. The non detection of ionized gas outflow in galaxies showing a molecular outflow is also found in other compact systems like NGC 1377 (Aalto et al. 2012). A comparison with other molecular outflows will be discussed in Section 4.

3.4. CO luminosity, H_2 mass and HCO^+/HCN upper limits

Figure 8 displays the total CO(3-2) spectrum, integrated over the entire observed map after correction for primary beam attenuation. When integrated over the line (FWHM=85.3 km/s), the integrated emission is 234± 1 Jy km/s. Towards the central position, Bajaja et al. (1995) found a CO(1-0) spectrum peaking at T_A^*= 48mK, with FWHM=168 km/s, yielding a total integrated flux of 193 Jy km/s, in a beam of 43″. Unfortunately, no CO(2-1) spectra have been reported. We can however remark that the CO(1-0) flux corresponds to a larger region than the one observed here (as witnessed by the broader linewidth), and our CO(3-2) flux is an upper limit of the expected CO(1-0) flux in a 18″ beam, since at low J the flux increases with the J-level. We can therefore safely conclude that the CO(3-2)/CO(1-0) ratio must be significantly larger than 2 in flux density units: the CO gas is relatively excited, meaning that the average density is at least of the order of 10^4 cm^{-3}. Assuming a CO(3-2)/CO(1-0) flux ratio of ~5, similar to that observed in the star-forming nuclei of nearby galaxies (e.g. Matsushita et al. 2004, Boone et al. 2011), the CO detected inside our primary beam, at the distance of 9.9 Mpc, corresponds to a molecular mass M(H_2) = 5.2 10^7 $M_\odot$, with the standard CO-to-H_2 conversion factor of 2.3 10^{20}cm^{-2}/(Kkm/s). By comparison, Bajaja et al. (1995) find in their central 43″ beam a mass of 1.8 10^8 $M_\odot$, covering an area 5.7 larger.

As far as the CO outflow is concerned, the use of any CO-to-H_2 conversion factor is uncertain. Let us then try to get a strict minimum of the mass in using the hypothesis of optically thin emission. Within this hypothesis, we can write the column density of CO in the upper state of the (3-2) transition as:

$$N_{J=3} = 6.410^{13} I_{CO(3-2)}$$

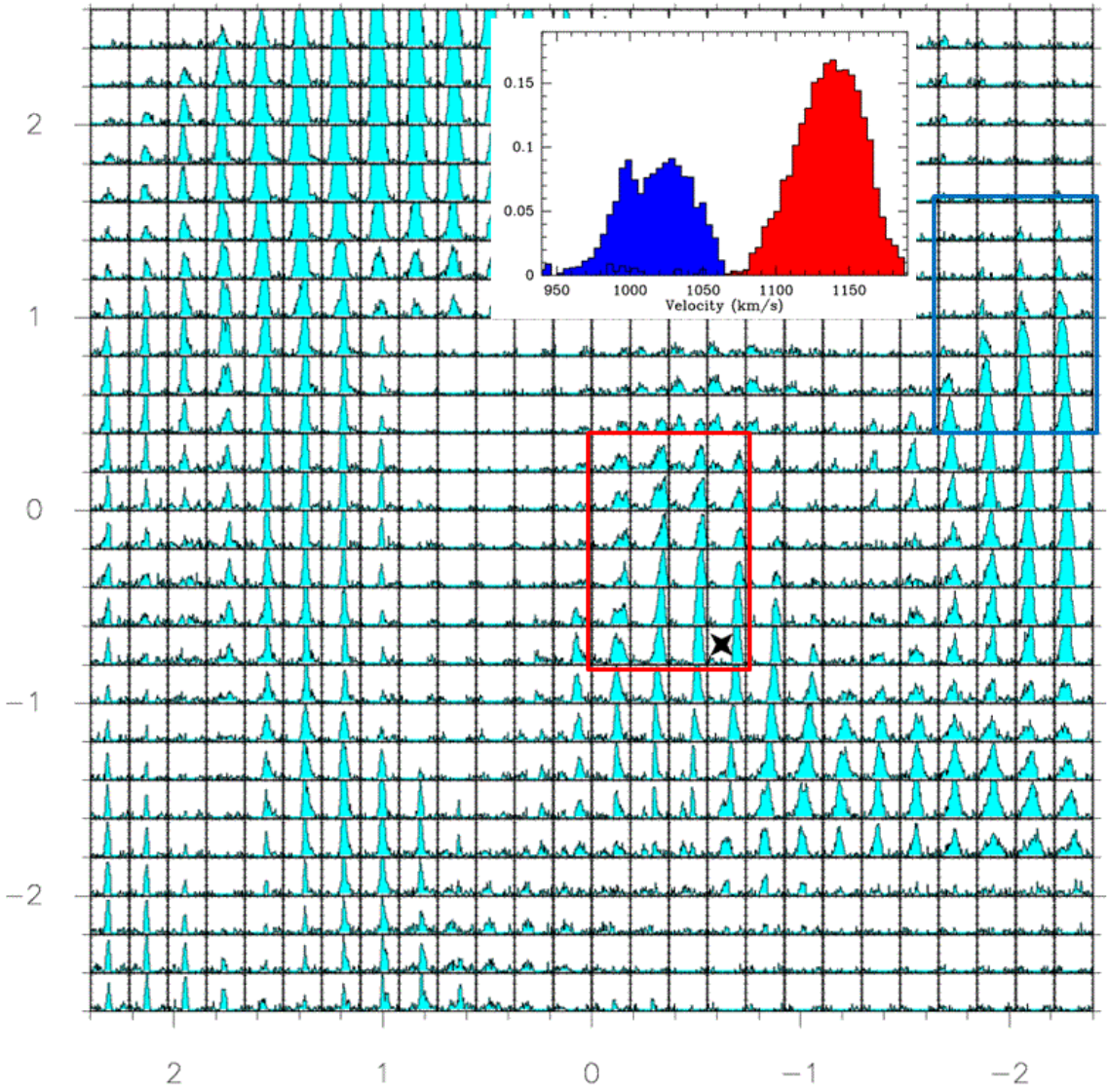

Fig. 9. CO(3-2) spectra within 2.″5 of the center. The velocity scale is from 960 to 1190 km/s (corresponding to -115 to 115 km/s with respect to the systemic velocity). The vertical scale is from 1 to 40 mJy. The new adopted center is marked with a black star (the map coordinates are with respect to the phase center). The red velocity component can be seen at the new center and just above, and the blue velocity component is centered at (-2, 0.5). The two regions 0.″7×1.″2 each, selected to integrate the outflow mass in Table 3 are indicated by red and blue rectangles respectively. The corresponding integrated spectra are plotted in the insert (scale in Jy).

where $I_{CO(3-2)}$ is the integrated (3-2) emission in K.km/s. The total CO column density is then obtained, using the ratio

$$N_{J=3}/N_{CO} = \frac{5}{Q} exp(-E_{J=3}/kT_{ex})$$

where $E_{J=3}$ is the energy in the upper level of the (3-2) transition, Q the partition function = 0.36 T_{ex}, and T_{ex} the excitation temperature, assumed constant over all J levels. The N(H_2) column density is then derived, assuming a CO abundance of 6 10^{-5} (e.g. Glover & Mac Low 2011). Comparing the N(H_2) values obtained within the optically thick hypothesis, and the use of the standard conversion factor, we found column densities less by factors 27, 71 and 83 when T_{ex}= 10, 20 and 30K respectively. Over the red outflow region large as 3-4 beams, we found N(H_2) ~ 5 10^{22} cm^{-2}, while the optically thin hypothesis will lead to values as low as 6 10^{20} cm^{-2}. We estimate that such low values are not realistic, however, since the mean volumetric density over the region will be ~ 1 cm^{-3}, and not 100 cm^{-3}, the minimum required to excite CO emission. Note that the mean CO(3-2) brightness temperature observed within the flow region if 3K, so that the surface filling factor of the molecular component cannot be much smaller than 0.1. Since the critical density of the CO(3-2) line is 10^5 cm^{-3}, the optically thin hypothesis is very unlikely to provide any emission, even taking into account the surface filling factor.

Finally, our simultaneous observations of HCO^+(4-3) and HCN(4-3) yielded only negative results. We can better derive significant upper limits towards the CO emission maxima. Over the whole map, there were 160 pixels (equivalent to 8 beams) with CO(3-2) emission larger than 60 times the 3σ upper limits in HCO^+(4-3) and HCN(4-3), assuming the same linewidth. In all CO maxima, an intensity ratio between CO and the high-density tracers >60 means that the average density of the gas in the multiple-arm flocculent spiral is not high. The critical density to excite the HCO^+(4-3) and HCN(4-3) molecular lines is at least 10^7 cm^{-3}.

4. Discussion and summary

We have presented our first ALMA results for a Seyfert 2 galaxy from our extended NUGA sample, NGC 1433. The observations in CO(3-2) allow us to reach an unprecedented spatial resolution of 24 pc, even with the limited Cycle 0 capabilities.

The morphology of the CO emission comes as a surprise. Although the Seyfert 2-type would suggest the presence of a thick obscuring component in front of the nucleus, there is no large concentration of molecular gas in the center, but instead a widely distributed multiple-arm spiral of CO emission, all over the nuclear ring region. The dense gas tracers HCO^+ and HCN remain undetected, confirming the absence of very dense gas (density larger than 10^7 cm^{-3}).

Although infrared images reveal the presence of a stellar nuclear bar inside the nuclear ring (of radius 0.5 kpc), located near the inner Lindblad resonances (e.g. Buta et al. 2001), the gas does not follow the nuclear bar. Instead the gas appears to flow inward and partly accumulate in a ring-like structure at a radius ~ 200 pc, which coincides with the inner ILR (IILR) as computed by Buta et al. (2001). This is indeed expected at some epochs of self-consistent N-body+hydro simulations, when the gas enters an inflowing phase inside two ILRs (e.g. Hunt et al. 2008). The gas is not stalled in this pseudo-ring, but continues to flow in towards the very center.

The kinematics of the CO emission are dominated by a rather regular rotational velocity field, with only slight perturbations from the multiple-arm spiral. No strong streaming motion is imprinted on these kinematics by the primary and nuclear bars, since their axes coincide with the galaxy major axis. Additionally, two peculiar features appear at high velocity, one red-shifted component towards the center within 100 pc, and a blue-shifted counterpart at 2″ (100 pc) from the center. The amplitude of these components is up to about 100 km/s in projection (~ 200 km/s if in the galaxy plane). Given their location near the nucleus, we tentatively interpret these high-velocity features as the two sides of an outflow. Globally, these features represent as much as ~ 7% of the total molecular emission, in the nuclear ring region, i.e., 3.6 x 10^6 M$_\odot$.

It is not likely that these peculiar high-velocity features reflect strong streaming motions due to a dynamical perturbation, since there is no such perturbation in the center. The gas is not following the nuclear bar, which is rather weak. Is a central mass able to generate such a high rotation in the center? Considering that the blue and red components are separated in projection along the minor axis by 2″= 100 pc, or about 120 pc in the plane of the galaxy, a massive black hole located in the center, at R=60pc from each component, should have a mass of at least M_{BH}=V^2 R/G, for the rotational velocity in the galaxy plane V=200km/s, or M_{BH}=5.6 10^8 M$_\odot$. This would make NGC 1433 a strong outlier to the $M_{BH} - \sigma$ relation; indeed from the bulge mass, we would expect the BH mass to be 5 10^6 M$_\odot$, e.g., Buta (1986). In any case, for gas rotating in circular motion, within the sphere of influence of the black hole, the velocity maxima should appear on the major axis and disappear on the minor axis, contrary to what is observed here. Another solution would be to assume the existence of a mini-polar disk, with completely different orientation than the main disk, and almost edge-on, but no galaxy interaction or accretion event support this hypothesis.

The origin of the outflow might be related to star formation, which is concentrated in the nuclear ring region. The star formation rate (SFR) can be estimated from the far infrared luminosity, as calibrated by Kennicutt (1998). From the IRAS fluxes, the FIR luminosity is 1.3 10^9 L$_\odot$ (Table 1), and the SFR equals 0.2 M$_\odot$/yr. From the Hα luminosity, measured at 3.7 10^{40} erg/s by Hameed & Devereux (2005), we can also deduce from Kennicutt's calibration, a SFR = 0.29 M$_\odot$/yr, which is quite compatible.

The order of magnitude of the mass outflow rate can be computed, using our estimates for the molecular mass in the high-velocity components (Table 3), as M=3.6 10^6 M$_\odot$. This mass has been obtained using the standard CO-to-H_2 conversion factor, since there is no reason a priori to adopt the lower factor applying to ULIRGs. Cicone et al. (2012) show in Mrk231 that the molecular gas in the galaxy and the outflowing gas share the same excitation. However, this mass could be an upper limit, if the flow is made of more diffuse gas. Since each high-velocity component has a projected radial extent from the center of d=1″ ~ 50 pc, and moves at a projected velocity of v=100 km/s, the flow rate is of the order of dM/dt ~ (Mv/d) tanα= 7 tanα M$_\odot$/yr, with α being the angle between the outflow and the line of sight.

Although this estimate is uncertain by a factor of a few, given the unknown α, it is about 40 times higher than the SFR; since galactic winds due to starbursts correspond in general to mass outflows of the same order as the SFR (e.g. Veilleux et al. 2005), we conclude that the outflow is not likely due to star formation alone, and is at least helped by the AGN. We note that starburst winds are generally observed in galaxies with SFR larger than 5 M$_\odot$/yr, and SFR surface densities larger than 10^{-3} M$_\odot$/yr/kpc^2. NGC 1433 has a low total SFR ~ 0.2 M$_\odot$/yr, however, its SFR surface density is 0.34 M$_\odot$/yr/kpc^2, if we assume that the whole SFR is confined to the nuclear disk of 9″radius. The SFR surface density would therefore be enough to drive a wind, although (as noted above) the mass loading factor expected for this type of wind would still be considerably lower than what we observe in NGC 1433.

The kinetic luminosity of the flow can be estimated as L_{kin} =0.5 dM/dt v^2 =2.3 tanα (1+ tan$^2\alpha$) 10^{40} erg/s. The luminosity of the AGN can be estimated at various wavelengths. Although the X-ray point source is weak, 1.7 10^{39} erg/s over 0.3-8kev (Liu & Bregman 2005), we can derive a bolometric luminosity of the AGN from optical and NIR magnitudes in the central aperture (Buta et al. 2001) of 1.3 10^{43} erg/s. From the expected BH mass of 5 10^6 M$_\odot$, if NGC 1433 is on the $M_{BH} - \sigma$ relation, the Eddington luminosity is 6.3 10^{44} erg/s. The kinetic luminosity of the outflow is low with respect to the bolometric luminosity of the AGN, making it plausible that the latter is able to power the wind.

The momentum flux of the outflow, computed by dM/dt v is however too large with respect to that provided by the AGN photons L_{AGN}/c, by a factor 2000 tanα/cosα. Although the momentum can be boosted in case of energy-conserved wind by factors up to 50 (e.g. Faucher-Giguère & Quataert 2012), it is more likely that the AGN contributes to drive the outflow not by its radiation pressure, but through its radio jets. From the central 1.4 GHz power of 3.4mJy detected by Ryder et al. (1996), we can estimate the jet power, from the formula proposed by Birzan et al. (2008, their equation 16): P_{jet} = 2 10^{42} erg/s. Since this power is about two orders of magnitudes higher than the kinetic luminosity of the outflow, the jet is amply able to drive the flow, even with low coupling. The jet interaction with the interstellar medium has been simulated by Wagner et al. (2012) who show that the jet is able to drive a flow efficiently, as soon as the Eddington ratio of the jet P_{jet}/L_{Edd} is larger than 10^{-4}. In NGC 1433, this ratio is about 3.2 10^{-3}.

The molecular outflow in NGC 1433 is one of only a few discovered recently occuring in low-star forming galaxies, with relatively weak AGN, where the flow might be driven by both

the starburst and the radio jets. The LINER NGC 6764 has 4.3 10^6 $M_\odot$ of molecular gas driven out with a velocity of about 100 km/s (Leon et al. 2007). The flow projects to larger distances than in NGC 1433, and might be more evolved. The outflow rate is lower, of the order of 1 $M_\odot$/yr. NGC 1266 is also a LINER and has the highest flow rate of 13 $M_\odot$/yr, with 2.4 10^7 $M_\odot$ of molecular gas driven with V=177 km/s (Alatalo et al. 2011). A third LINER, with total SFR of ~ 1 $M_\odot$/yr, NGC 1377 has an outflow rate of 8 $M_\odot$/yr, an outflowing mass of 1.1 10^7 $M_\odot$, at V=140 km/s (Aalto et al. 2012). All these galaxies have star formation playing a role in the outflow, but the properties of the flow require the contribution of the AGN, through the entrainement of its radio jets. The latter is the most needed for NGC 1433, which has the lowest SFR of all.

This tentative detection of a molecular gas outflow, triggered essentially by the AGN, should be confirmed by higher-resolution ALMA observations. The detection of a radio continuum component at the very center, which might be due to thermal dust emission from a molecular torus, also deserves a higher-resolution study.

Acknowledgements. We warmly thank the referee for constructive comments and suggestions. The ALMA staff in Chile and ARC-people at IRAM are gratefully acknowledged for their help in the data reduction. We particularly thank Gaelle Dumas and Philippe Salomé for their useful advice. We used observations made with the NASA/ESA Hubble Space Telescope, and obtained from the Hubble Legacy Archive, which is a collaboration between the Space Telescope Science Institute (STScI/NASA), the Space Telescope European Coordinating Facility (ST-ECF/ESA) and the Canadian Astronomy Data Centre (CADC/NRC/CSA). F.C. acknowledges the European Research Council for the Advanced Grant Program Num 267399-Momentum. I.M. acknowledges financial support from the Spanish grant AYA2010-15169 and from the Junta de Andalucia through TIC-114 and the Excellence Project P08-TIC-03531. We made use of the NASA/IPAC Extragalactic Database (NED), and of the HyperLeda database.

References

Aalto S., Muller S., Sakamoto K. et al. 2012, A&A 546, A68
Alatalo K., Blitz L., Young L.M. et al. 2011, ApJ, 735, 88
Bajaja E., Wielebinski R., Reuter H.P. et al. 1995, A&AS, 114, 147
Birzan L., McNamara B.R., Nulsen P.E.J. et al. 2008, ApJ 686, 859
Boone F., Garcia-Burillo S., Combes F. et al. 2011, A&A, 525, A18
Buta R. 1986, ApJS 61, 631
Buta R., Combes F. 1996, Fundamentals of Cosmic Physics 17, 95
Buta R., Combes F. 2000, in ASP. Conf. Ser. 197, Dynamics of Galaxies: From the Early Universe to the Present, ed. F. Combes, G. A. Mamon, & V. Charmandaris (San Francisco ASP), 11
Buta, R., Ryder, S. D., Madsen, G. J., Wesson, K., Crocker, D. A., Combes, F. 2001, AJ, 121, 225
Casasola, V., Combes, F., Garcia-Burillo, S. 2008, A&A, 490, 61
Casasola, V., Hunt, L. K., Combes, F., Garcia-Burillo, S., Neri, R. 2011, A&A, 527, A92
Chung, A., Yun, M. S., Naraynan, G., Heyer, M., Erickson, N. R. 2011, ApJ, 732, L15
Cicone C., Feruglio C., Maiolino R. et al. 2012, A&A 543, A99
Coil, A. L., Weiner, B. J., Holz, D. E., et al. 2011, ApJ, 743, 46
Combes F. 2003 ASP Conf Series, 290. 411
Combes F. 2006 Astrophysics Update 2, Springer, p.159
Comeron, S., Knapen, J. H., Beckman, J. E. et al. 2010, MNRAS, 402, 2462
Croton, D. J., Springel, V., White, S. D. M. et al. 2006, MNRAS, 365, 11
Dasyra, K., Combes, F.: 2012, A&A 541, L7
Di Matteo, T., Colberg, J., Springel, V., Hernquist, L., Sijacki, D. 2008, ApJ, 676, 33
Draine B.T., Lee H.M. 1984, ApJ, 285, 89
Dumke M., Braine J., Krause M. et al. 1997, A&A, 325, 124
Faucher-Giguère C.-A., Quataert E. 2012, MNRAS 425, 605
Feruglio, C., Maiolino, R., Piconcelli, E., et al. 2010 A&A, 518, L155
Feruglio, C., Fiore, F., Piconcelli, E., et al. 2013, A&A, 549, A51
Fischer, J., Sturm, E., Gonzalez-Alfonso, E. et al. 2010, A&A 518, L41
Friedli D., Martinet L. 1993, A&A 277, 27
Galliano E., Aloin D. 2002 A&A, 393, 43
Garcìa-Burillo, S., Fernandez-Garcia S., Combes F. et al. 2009, A&A, 496, 85
Garcìa-Burillo, S., Usero, A., Fuente, A. et al. 2010, A&A, 519, A2
Glover, S. C. O., Mac Low, M.-M., 2011, MNRAS 412, 337
Guilloteau, S., Lucas, R. 2000, Imaging at Radio through Submillimeter Wavelengths, 217, 299, 10
Hameed S., Devereux N. 2005, AJ, 129, 2597
Harnett J.I. 1987, MNRAS, 227, 887
Ho, L. C., Li, Z-Y, Barth, A. J. et al. 2011, ApJS, 197, 21
Hopkins, P.F., Quataert, E.2010, MNRAS, 407, 1529
Hopkins, P., Hernquist, L., Cox, T.J. et al. 2006, ApJS, 163, 1
Hunt L.K., Malkan M.A. 1999, ApJ, 516, 660
Hunt, L. K., Combes F., Garcia-Burillo S. et al. 2008, A&A, 482, 133
Jogee S. 2006 Lecture Notes in Physics 693, 143
Jungwiert B., Combes F., Axon D.J. 1997, A&AS, 125, 479
Kennicutt R.C. 1998, ApJ, 498, 541
Kilborn, V. A., Koribalsi B.S., Forbes, D.A. et al. 2005, MNRAS 356, 77
Kormendy J., Ho L.C. 2013, ARAA in press, arXiv:1308.6483
Krips M., Martin, S., Eckart, A. et al. 2011, ApJ, 736, 37
Leon S., Eckart A., Laine S. et al. 2007, A&A 473, 747
Lindt-Krieg, E., Eckart, A., Neri, R. et al. 2008, A&A, 479, 377
Liu J-F., Bregman J.N.: 2005, ApJS 157, 59
Malkan M., Gorjian V., Tam R. 1998, ApJS, 117, 25
Maoz, D., Barth, A. J., Sternberg, A., et al. 1996, AJ, 111, 2248
Matsushita S., Sakamoto K., Kuo C-Y. et al. . 2004, ApJ, 616, L55
McMullin, J. P., Waters, B., Schiebel, D., Young, W., Golap, K. 2007, Astronomical Data Analysis Software and Systems XVI, 376, 127
Müller Snchez, F., Davies, R. I., Genzel, R. et al. 2009, ApJ, 691, 749
Nesvadba, N. P. H., Polletta, M., Lehnert, M. D. et al. 2011, MNRAS 415, 2359
Peeples, M. S., Martini, P. 2006, ApJ, 652, 1097
Perez-Beaupuits, J.,Wada, K., Spaans, M.2011, ApjJ, 730, 48
Piner, B.G., Stone, J.M., Teuben, P.J. 1995, ApJ, 449, 508
Regan, M.W., Teuben, P.J. 2004, ApJ, 600, 595
Riffel R.A., Storchi-Bergmann T. 2011, MNRAS, 411, 469
Roussel, H., Vigroux, L., Bosma, A. et al. 2001, A&A 369, 473
Rupke, D. S., Veilleux, S., Sanders, D. B.2005, ApJ, 632, 751
Ryder, S. D., Buta, R. J., Toledo, H. 1996, ApJ, 460, 665
Sadler E.M., Slee O.B., Reynolds J.E., Roy A.L. 1995, MNRAS, 276, 1373
Sakamoto K, Aalto S., Wilner D. et al. 2009, ApJ, 700, L104
Schinnerer, E., Eckart, A., Tacconi, L. J., Genzel, R., Downes, D. 2000, ApJ, 533, 850
Solomon P.M., Vanden Bout P.A. 2005, ARAA, 43, 677
Sosa-Brito, R. M., Tacconi-Garman, L. E., Lehnert, M. D., Gallimore, J. F. 2001, ApJS, 136, 61
Spoon H.W.W., Farrah D., Lebouteiller V. et al. , 2013, ApJ sub (arXiv1307.6224)
Stil J.M., Krause M., Beck R., Taylor A.R. 2009, ApJ, 693, 1392
Sturm, E., Gonzalez-Alfonso, E., Veilleux, S. et al. 2011, ApJ, 733, L16
Treuthardt P., Salo H., Rautiainen P., Buta R. 2008, AJ, 136, 300
Ulvestad, J. S., Ho, L. C. 2001, ApJ, 558, 561
Veilleux S., Cecil G., Bland-Hawthorn J.: 2005, ARAA 43, 769
Veilleux S., Melendez M., Sturm E. et al. 2013, ApJ sub (arXiv1308.3139)
Veron-Cetty, M.P., Veron, P. 1986, A&AS, 66, 335
Wagner A.Y., Bicknell G.V., Umemura M. 2012, ApJ 757, 136